The Astrophysical Journal, 835:42 (7pp), 2017 January 20 doi:10.3847/1538-4357/835/1/42

HESS J1427−608: AN UNUSUAL HARD, UNBROKEN γ-RAY SPECTRUM IN A VERY WIDE ENERGY RANGE

Xiao-Lei Guo[1,2], Yu-Liang Xin[2,3], Neng-Hui Liao[2], Qiang Yuan[2], Wei-Hong Gao[1], Hao-Ning He[2], Yi-Zhong Fan[2], and Si-Ming Liu[2]
[1] Department of Physics and Institute of Theoretical Physics, Nanjing Normal University, Nanjing 210046, China; yuanq@pmo.ac.cn, gaoweihong@njnu.edu.cn, liusm@pmo.ac.cn
[2] Key Laboratory of Dark Matter and Space Astronomy, Purple Mountain Observatory, Chinese Academy of Sciences, Nanjing 210008, China
[3] University of Chinese Academy of Sciences, Yuquan Road 19, Beijing, 100049, China
Received 2016 September 7; revised 2016 November 27; accepted 2016 November 28; published 2017 January 17

ABSTRACT

We report the detection of a GeV γ-ray source that spatially overlaps and is thus very likely associated with the unidentified very high energy (VHE) γ-ray source HESS J1427−608 with the Pass 8 data recorded by the *Fermi Large Area Telescope*. The photon spectrum of this source is best described by a power law with an index of 1.85 ± 0.17 in the energy range of 3–500 GeV, and the measured flux connects smoothly with that of HESS J1427−608 at a few hundred gigaelectronvolts. This source shows no significant extension and time variation. The broadband GeV to TeV emission over four decades of energies can be well fitted by a single power-law function with an index of 2.0, without obvious indication of spectral cutoff toward high energies. Such a result implies that HESS J1427−608 may be a PeV particle accelerator. We discuss the possible nature of HESS J1427−608 according to the multiwavelength spectral fittings. Given the relatively large errors, either a leptonic or a hadronic model can explain the multiwavelength data from radio to VHE γ-rays. The inferred magnetic field strength is a few micro-Gauss, which is smaller than the typical values of supernova remnants (SNRs) and is consistent with some pulsar wind nebulae (PWNe). On the other hand, the flat γ-ray spectrum is slightly different from typical PWNe but is similar to that of some known SNRs.

Key words: gamma rays: general – gamma rays: ISM – ISM: individual objects (HESS J1427−608) – ISM: supernova remnants – radiation mechanisms: nonthermal

1. INTRODUCTION

The High Energy Stereoscopic System (HESS) survey of the inner Galaxy (Aharonian et al. 2006a) has discovered a large number of very high energy (VHE; >100 GeV) sources. About half of them have been firmly identified as supernova remnants (SNRs) and pulsar wind nebulae (PWNe). However, there are still a significant fraction of VHE sources that have not been identified due to the lack of counterparts in the radio/X-ray or GeV γ-ray bands (Aharonian et al. 2005, 2008a). Therefore, searching for the counterparts of these unidentified VHE sources in longer-wavelength bands is very helpful to identify and classify them. In the GeV band, more than 7 years of survey data from the *Fermi Large Area Telescope* (*Fermi*-LAT) provides a good opportunity to hunt for the unidentified VHE sources. Indeed, several unidentified VHE sources have been detected with the *Fermi*-LAT data (Hui et al. 2016).

HESS J1427−608 is one of the unidentified VHE sources discovered by the HESS Galactic Plane Survey (Aharonian et al. 2008a). The TeV image shows that it is only slightly extended with a symmetric Gaussian function with a width of $\sigma = 3'$. This source is detected with an integral flux above 1 TeV of $F_\gamma(>1\,\mathrm{TeV}) = 4.0 \times 10^{-12}\,\mathrm{erg\,cm^{-2}\,s^{-1}}$ and a power-law spectrum with an index of $\Gamma = 2.16$. No nearby SNR or pulsar was detected in the vicinity of HESS J1427−608 (Green 2014). The X-ray counterpart of it, Suzaku J1427−6051, was reported by Fujinaga et al. (2013). The X-ray spatial morphology is clearly extended with a Gaussian width of $\sigma = 0.'9 \pm 0.'1$, and the spectrum is well fitted by a power law with an index of $\Gamma = 3.1^{+0.6}_{-0.5}$, implying nonthermal X-ray continuum emission. The unabsorbed flux in the 2–10 keV band is $F_X = (9^{+4}_{-2}) \times 10^{-13}$ erg cm^{-2} s^{-1}. Fujinaga et al. (2013) have discussed the possible nature of HESS J1427−608 as a PWN or nonthermal SNR. Each one can explain some of the observational facts but face difficulties. No radio counterpart was detected in the direction of HESS J1427−608. In the second *Fermi*-LAT catalog (2FGL; Nolan et al. 2012), a GeV source, 2FGL J1427.6−6048c, which is located in the vicinity of HESS J1427−608, was reported. However, their central positions differ moderately from each other. Furthermore, the power-law spectrum index of 2FGL J1427.6−6048c is $\Gamma = 2.7$ (Nolan et al. 2012), which cannot connect with the TeV spectrum of HESS J1427−608 well. It is very likely that 2FGL J1427.6−6048c is not associated with HESS J1427−608. Meanwhile, it should be noted that no source in the third *Fermi*-LAT source catalog (3FGL; Acero et al. 2015) is associated with 2FGL J1427.6−6048c.

In this paper, we carry out a complete analysis of this region using more than 7 years of *Fermi*-LAT Pass 8 data to investigate the γ-ray emission of HESS J1427−608. In Section 2, we describe the data analysis and results, including the spatial, spectral, and timing analyses. The possible nature of HESS J1427−608 based on the multiwavelength spectral energy distribution (SED) fitting is discussed in Section 3, and the conclusion of this work is presented in Section 4.

2. DATA ANALYSIS

2.1. Data Reduction

The following analysis is performed using the latest *Fermi*-LAT Pass 8 data with the *Source* event class from 2008 August 4 (Mission Elapsed Time 239557418) to 2015 November 4 (Mission Elapsed Time 468288004). Considering the impact of the point-spread function (PSF) and the complex diffuse emission from the Galactic plane, we only select events with

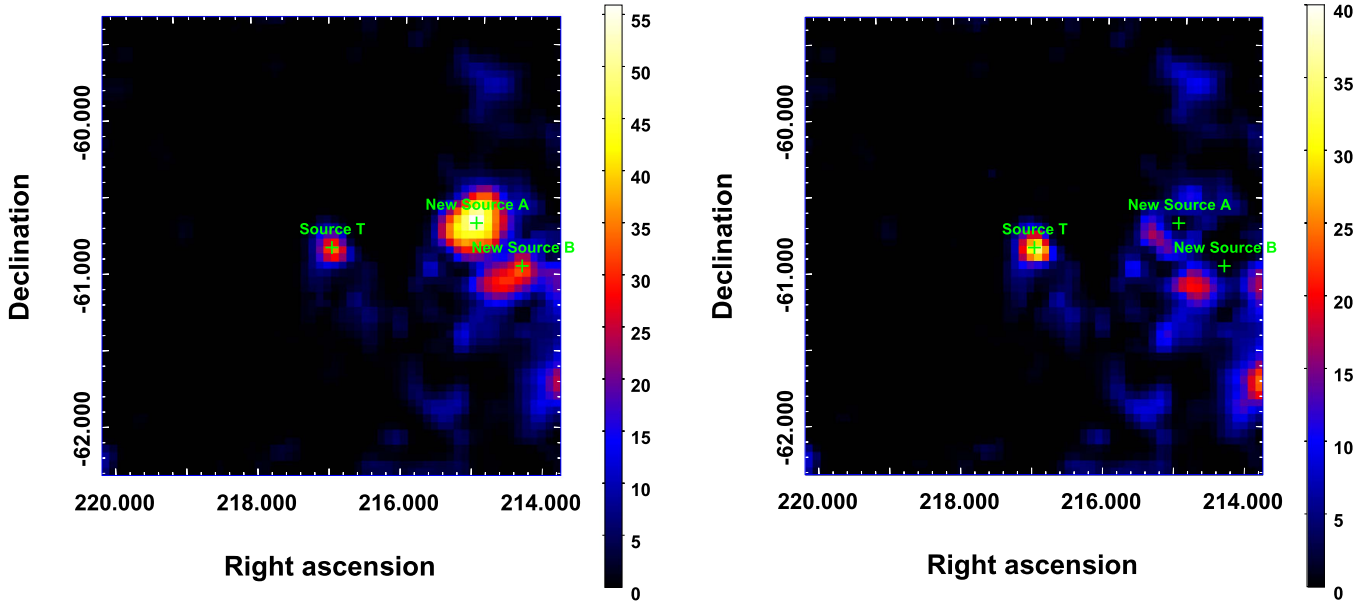

Figure 1. TS maps of the 3° × 3° region centered at HESS J1427−608 for photons above 3 GeV. The left-hand panel is for the standard model where contributions from 3FGL sources and diffuse backgrounds have been subtracted. The green crosses denote the newly added sources listed in Table 1. The right panel is the TS map with the additional New Sources A and B subtracted. All maps are smoothed with a Gaussian kernel of $\sigma = 0.^{\circ}1$.

energies between 3 GeV and 500 GeV. Furthermore, in order to reduce the contamination from the Earth limb, the events with zenith angles larger than 90° are excluded. The region of interest (ROI) we analyze is a 14° × 14° square region centered at the position of HESS J1427−608 (R.A. = $216.^{\circ}967$, Decl. = $-60.^{\circ}85$; Aharonian et al. 2008a). We analyze the data using the *Fermi ScienceTools* version `v10r0p5`[4] and the instrument response function (IRF) of P8R2_SOURCE_V6. To model the Galactic diffuse emission and isotropic diffuse background, `gll_iem_v06.fits` and `iso_P8R2_SOURCE_V6_v06.txt`[5] are adopted. In addition to the diffuse backgrounds, the sources included in the 3FGL and located within the ROI are added to the model to account for γ-ray emission. In the following analysis, the standard binned likelihood method with `gtlike` is applied.

2.2. Source Detection

In each `gtlike` run, the normalizations and spectral parameters of sources with distance smaller than 7° to HESS J1427−608, as well as the normalizations of the two diffuse backgrounds, are left free during the fitting. After including in the sky model the emission from 3FGL sources and the two diffuse backgrounds, we create a 3° × 3° test statistic (TS) map centered at HESS J1427−608 with `gttsmap`, as shown in the left-hand panel of Figure 1. As can be seen from this TS map, there are still some significant excesses (marked by green crosses) that are not included in the model. In particular, there are some complicated excesses to the west of the ROI center, which we mark as New Source A and B. These excesses are spatially consistent with the two "wings" of the Kookaburra complex (HESS J1420−607 & HESS J1418−609; Aharonian et al. 2006b). The two "wings" are two extended γ-ray sources and are argued to be PWN candidates by Aharonian et al. (2006b). Acero et al. (2013) explored high-energy γ-ray emission from these two sources with *Fermi*-LAT and concluded that HESS J1420−607 was a PWN candidate, and the emission from HESS J1418−609 was dominated by a pulsar. Besides the New Source A and B, we find an significant excess at the ROI center, the position of HESS J1427−608. This source, referred as Source T, is the focus of this work. These three new sources are added to the model as point sources with power-law spectra. Their accurate positions are obtained with the `gtfindsrc` command. Their resulting coordinates and TS values are listed in Table 1. The new TS map with sources A and B included in the model (and hence subtracted from the map) is shown in the right-hand panel of Figure 1. Except for Source T, this TS map is relatively clean with only small residuals.

Table 1
Coordinates and TS Values of the New Point Sources

Name	R.A. (deg)	Decl. (deg)	TS
Source T	216.960	−60.8595	40
New Source A	215.028	−60.6853	63
New Source B	214.396	−60.9555	34

Now we mainly discuss Source T. Source T is detected with a TS value of 40, which corresponds to a significance of $\sim 5.5\sigma$ for four degrees of freedom (dof). The best-fitting position of Source T is R.A. = $216.^{\circ}960$, Decl. = $-60.^{\circ}8595$ with 1σ error circle of $0.^{\circ}018$. The distance between Source T and the central position of HESS J1427−608 is only $0.'7$, within the 1σ error circle of the *Fermi*-LAT data. To better understand the spatial correlation between Source T and HESS J1427−608, as well as candidate counterparts in other wavelengths, we create a zoom-in TS map for a region of $0.^{\circ}5 \times 0.^{\circ}5$ centered at Source T, as shown in Figure 2. The position and extended size of HESS J1427−608 (Aharonian et al. 2008a), as well as the X-ray counterpart Suzaku J1427−6051 (Fujinaga et al. 2013), are overplotted. As we can see from Figure 2, Source T is well coincident with HESS J1427−608 and Suzaku J1427−6051.

[4] http://fermi.gsfc.nasa.gov/ssc/data/analysis/software/
[5] http://fermi.gsfc.nasa.gov/ssc/data/access/lat/BackgroundModels.html

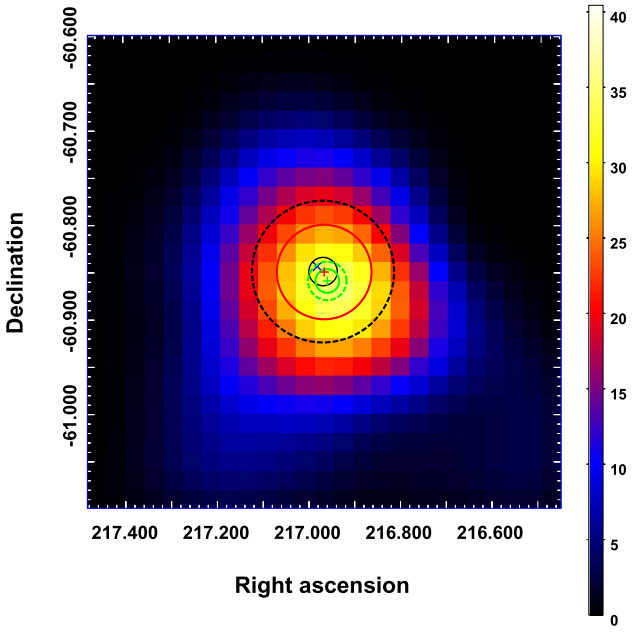

Figure 2. TS map above 3 GeV for a region of $0.^{\circ}5 \times 0.^{\circ}5$ centered at the best-fit position of Source T. The pixel size is $0.^{\circ}02 \times 0.^{\circ}02$, and smoothing is applied with a Gaussian function of $\sigma = 0.^{\circ}04$. The green plus sign denotes the best-fitting position of Source T. The 1σ and 2σ positional error circles of Source T are marked by green solid and dashed circles, respectively. The position of HESS J1427−608 is marked with a red plus sign, and the red circle represents the extended morphology with a radius of $\sigma = 3'$ (Aharonian et al. 2008a). The black solid circle shows the core region of Suzaku J1427−6051 with an extension of $\sigma = 0.'9$, and the source region with a radius of $4.'5$ defined in Fujinaga et al. (2013) is indicated by the dashed circle. A radio source named MGPS J142755−605038 in this region observed in the second-epoch Molonglo Sky Survey (Murphy et al. 2007) is marked by the blue cross.

Therefore, Source T is very likely to be the GeV counterpart of HESS J1427−608.

2.3. Spatial Extension

Considering that HESS J1427−608 is slightly extended in the TeV and X-ray bands, we therefore reperform the analysis with three uniform disks with different radii to test its spatial extension. The radii of the three uniform disks we adopted are $0.^{\circ}1$, $0.^{\circ}15$, and $0.^{\circ}2$, and the best-fitting TS values are 35, 31, and 24, respectively. The larger the radius of the uniform disk, the smaller the TS value is. We also test the extension using the data with four PSF event types,[6] and we find no significant spatial extension of the γ-ray emission. Therefore, a point-like source is enough to explain the γ-ray emission of Source T. In the following sections, we treat Source T as a point source.

2.4. Spectral Analysis

To investigate the spectrum of Source T, we perform the global likelihood analysis in the energy range between 3 GeV and 500 GeV. The spectrum of Source T can be well described by a power law. The spectral index is 1.85 ± 0.17, and the integral photon flux is $(3.06 \pm 0.73) \times 10^{-10}$ photon cm^{-2} s^{-1} with statistical error only. Since no information on the distance of HESS J1427−608 is available yet, we assume that d is 8 kpc

[6] http://fermi.gsfc.nasa.gov/ssc/data/analysis/documentation/Cicerone/Cicerone_Data/LAT_DP.html

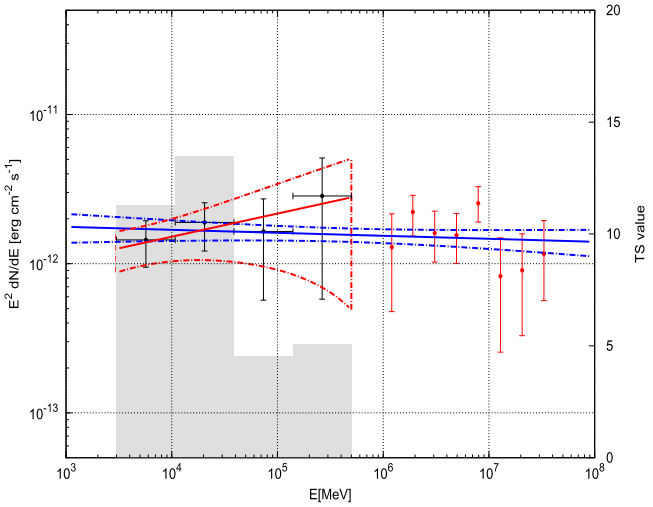

Figure 3. SED of Source T. The black dots depict the *Fermi*-LAT data in 3–500 GeV, and the high-energy data observed by HESS are marked as red dots (Aharonian et al. 2008a). The gray histogram shows the TS value of each energy bin. The red solid and dot-dashed lines indicate the best-fitting power-law spectrum and the 1σ statistical error for *Fermi*-LAT data in 3–500 GeV, respectively. A power-law spectrum with an index of 2.02 ± 0.03 for the global γ-ray data is plotted as the blue solid line, and its 1σ statistical error is also marked by the blue dot-dashed lines.

following Fujinaga et al. (2013). Thus the γ-ray luminosity above 3 GeV is $7.54 \times 10^{34}\ (d/8\ \mathrm{kpc})^2$ erg s^{-1}.

Then we bin the data into four logarithmically even energy bins from 3 to 500 GeV and repeat the likelihood fitting to give the SED. The spectral normalizations of all sources within 7° from Source T and the normalizations of the two diffuse backgrounds are set as free parameters, while the spectral indexes of these sources are fixed. The SED is plotted in Figure 3. As we can see from the SED, the *Fermi*-LAT data connect with HESS's TeV spectrum smoothly, which further supports that Source T is the GeV counterpart of HESS J1427−608.

2.5. Timing Analysis

To check out whether Source T is variable or not, the timing analysis is performed. We bin the data into seven equal time bins. The analysis procedure is the same as the spectral analysis. For any time bin whose TS value is smaller than 4, the 95% upper limit is calculated. The light curve is shown in Figure 4. No obvious variability of Source T can be seen from this light curve. However, this may be partially due to the limited statistics of photons from the source. A further timing analysis with more data may be helpful in revealing its variable or steady nature.

3. DISCUSSION

3.1. Multiwavelength Observations

From the above analysis, Source T is positionally consistent with HESS J1427−608, and its spectrum also connects with the HESS observation smoothly, which all support that Source T is the GeV counterpart of HESS J1427−608.

The X-ray emission observed by *Suzaku* is identified to be nonthermal (Fujinaga et al. 2013). The unabsorbed flux in the 2–10 keV band is $\sim 9 \times 10^{-13}$ erg s^{-1} cm^{-2} with the 90% upper

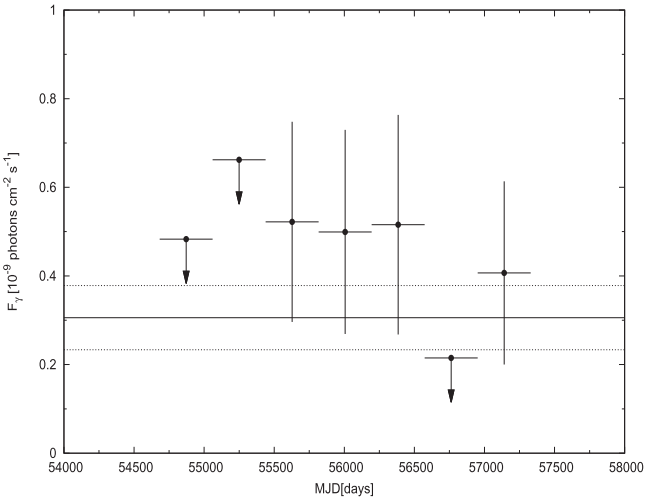

Figure 4. Light curve for Source T. The horizontal solid line represents the average flux from the whole data set whose 1σ uncertainty is marked by the two dotted lines.

limit in the 15–40 keV band of $\sim 5.3 \times 10^{-12}$ erg s^{-1} cm^{-2} (Fujinaga et al. 2013).

A radio compact source MGPS J142755−605038 with total flux density at 843 MHz of 34.5 mJy, discovered in the second-epoch Molongo Sky Survey (MGPS-2; Murphy et al. 2007), is located very close to HESS J1427−608. Vorster et al. (2013) treated it as the radio counterpart of HESS J1427−608. However, the morphology of the radio source is distinct from that of TeV γ-rays. Murphy et al. (2007) fitted the source morphology with a two-dimensional Gaussian function and obtained that the FWHM sizes of the major and minor axes (θ_M, θ_m) are 92.″4 and 66.″9, respectively. Such an extension is significantly smaller than that of the TeV γ-ray extension. Therefore we alternatively scale up the flux density of MGPS J142755−605038 by a factor of 29 (the area ratio of the TeV γ-ray to the radio morphologies) as a very loose upper limit of the radio emission of HESS J1427−608. The actual upper limit should be lower than such a result.

3.2. Radiation Mechanism

Here we consider two scenarios for the origin of γ-ray emission. In the leptonic scenario, the γ-ray emission can be produced by inverse Compton scattering (ICS) or a bremsstrahlung process of high-energy electrons. In the hadronic scenario, the γ-ray photons originate from the decay of neutral pion mesons produced in collisions between accelerated protons and the ambient materials. The *Fermi*-LAT results we get and the TeV γ-ray data observed by HESS will be used to study the multiwavelength SED of HESS J1427−608.

In the following, we quantitatively discuss the leptonic and hadronic scenarios with the multiwavelength data. In the modeling, a power-law spectrum with an exponential cutoff for electrons and protons is assumed: $dN/dE_i \propto E_i^{-\alpha_i} \exp(-E_i/E_{i,\rm cut})$, where $i = e, p$, α_i is the spectral index and $E_{i,\rm cut}$ is the cutoff energy. Besides the cosmic microwave background (CMB), the radiation field also includes an infrared blackbody component ($T_{\rm IR} = 30$ K, $U_{\rm IR} = 1$ eV cm^{-3}) and an optical blackbody component ($T_{\rm opt} = 6000$ K, $U_{\rm opt} = 1$ eV cm^{-3}) (Porter et al. 2006). The distance of HESS J1427−608 is taken to be 8 kpc, which follows the assumption in Fujinaga et al. (2013). The radius of HESS J1427−608 is ∼7 pc correspondingly. Here the gas density of $n_{\rm gas} = 1$ cm^{-3} is assumed.

3.2.1. Leptonic Scenario

For the leptonic scenario, all these fitted parameters are listed in Table 2, which are used to calculate the radiation spectrum as shown in the top panel of Figure 5. To explain the emission from radio to the TeV band, we get the model parameters of $\alpha_{\rm e} \approx 2.3$ and $E_{e,\rm cut} \approx 35$ TeV. While the radio flux upper limit favors a lower value of α_e, the γ-ray spectrum prefers a value of 3. A broken power-law model will lead to a better fit to the broadband SED, as shown in the top panel of Figure 5. However, if MGPS J142755−605038 is treated as the radio counterpart of HESS J1427−608, the spectrum of electrons should be harder, which makes it difficult to explain the flat spectrum in the γ-ray band. This will be a challenge to the leptonic scenario.

A very low strength of magnetic field, $B \approx 5.0\,\mu$G, is derived in order not to overproduce the synchrotron emission in the radio band in this scenario. This value is very close to the strength of the Galactic magnetic field. The total energy of electrons above 1 GeV is estimated to be $W_{\rm e} \approx 2.5 \times 10^{48} (d/8.0\,{\rm kpc})^2$ erg, which would vary with the value of distance adopted.

3.2.2. Hadronic Scenario

The fitted multiwavelength SED with hadronic scenario is compiled in the bottom panel of Figure 5, and the model parameters are listed in Table 2. In this model, the spectral indexes of protons and electrons are set equal to 2.0 in view of the diffusive shock acceleration mechanism, and the magnetic field strength is adopted to be a typical value of $B \approx 10\,\mu$G to reduce the number of free parameters in the model. Based on this, a cutoff energy of ∼30 TeV and a total energy above 1 GeV of $W_{\rm e} \approx 0.6 \times 10^{47}$ $(d/8.0\,{\rm kpc})^2$ erg for electrons are needed to explain the flux in the radio and X-ray bands. The total energy of protons above 1 GeV is $W_p \approx 1.0 \times 10^{51}$ $(n/1.0\,{\rm cm}^{-3})^{-1}$ $(d/8.0\,{\rm kpc})^2$ erg. However, this parameter strongly depends on the values of gas density and distance adopted here. Since there is no evident cutoff in the photon spectrum in the TeV energy band, the cutoff energy of protons should be larger than ∼350 TeV for the γ-ray spectrum with an index of 2.0 obtained above. For comparison, the π^0 decay component for protons without a high-energy cutoff is plotted in the bottom panel of Figure 2. HESS J1427−608 is a good candidate to accelerate cosmic ray (CR) protons up to several hundred TeV or even PeV energies. This is a good opportunity for the Cherenkov Telescope Array (CTA) to test the PeVatron (PeV CR accelerator) nature of HESS J1427−608. Note that for a distance of 8 kpc, the pair production absorption of the VHE photons by the infrared or CMB photons is nonnegligible (Zhang et al. 2006), and the extension of the power-law spectrum to PeV energies should be treated as an upper limit.

As can be seen in Figure 5, both the leptonic and hadronic models can fit the multiwavelength data of HESS J1427−608.

3.3. The Possible Nature of HESS J1427−608

Considering that most of the Galactic VHE sources are identified to be PWNe or SNRs, here we discuss these two possibilities as the origin of HESS J1427−608.

Table 2
Parameters for the Models

Model	α_p	α_e	$\Delta\alpha_e$	$E_{p,\mathrm{cut}}$ (TeV)	$E_{e,\mathrm{break}}$ (TeV)	$E_{e,\mathrm{cut}}$ (TeV)	W_p (10^{50} erg)	W_e (10^{48} erg)	B (μG)	n_{gas} (cm^{-3})
Leptonic (PL)	…	2.3	…	…	…	35.0	…	2.5	5.0	1.0
Leptonic (BPL)	…	1.6	1.0	…	0.1	80.0	…	3.0	3.5	1.0
Hadronic	2.0	2.0	…	350.0	…	30.0	10.0	0.06	10.0	1.0

Note. The total energy of relativistic particles, $W_{e,p}$, is calculated for $E > 1$ GeV.

3.3.1. SNR

First, we discuss the possibility that the emission comes from an SNR. For comparing between HESS J1427−608 and several of the most prominent SNRs, we plot their γ-ray SED in Figure 6. The energy fluxes of several SNRs are adjusted for the sake of illustration (Funk 2015), as shown in the legend of Figure 6. As can be seen, these SNRs can be divided into three classes. The first class is known to be interacting with molecular clouds, such as IC 443 (Abdo et al. 2010c; Ackermann et al. 2013), W44 (Abdo et al. 2010e; Ackermann et al. 2013), W51C (Abdo et al. 2009; Jogler & Funk 2016), W28 (Aharonian et al. 2008b; Abdo et al. 2010f), W49B (Abdo et al. 2010g; Brun et al. 2011), and CTB 37A (Brandt & Fermi-LAT Collaboration 2013; Zeng et al. 2016). These SNRs are old and typically brighter in the GeV than in the TeV band, and the γ-ray emissions of these sources are considered to be from the hadronic process. In particular, IC 443, W44, and W51C have shown the characteristic "π^0 bump" (Ackermann et al. 2013; Jogler & Funk 2016), which is considered to be the most direct evidence that protons are accelerated in SNRs. Differing from this class, the second class, such as RX J1713−3946 (Abdo et al. 2011; Yuan et al. 2011; Zeng et al. 2016), RX J0852−4622 (Tanaka et al. 2011), RCW 86 (Yuan et al. 2014), SN1006 (Acero et al. 2010; Araya & Frutos 2012; Xing et al. 2016), and CTB 37B (Xin et al. 2016; Zeng et al. 2016), has harder spectra in the GeV band and is brighter in the TeV band than in the GeV band. The sources in this class are middle-aged SNRs and are generally thought to have a leptonic origin for the γ-ray emission, although several of them are still being debated. The third class in Figure 6 includes Cas A (Abdo et al. 2010b; Yuan et al. 2013) and Tycho (Giordano et al. 2012; Morlino & Caprioli 2012; Zhang et al. 2013), which are the youngest SNRs. The γ-ray spectra of these two SNRs can be fitted by a power law extending from the GeV to the TeV band, which can be well explained as the hadronic emission. Like Cas A and Tycho, HESS J1427−608 also has a flat γ-ray spectra from gigaelectronvolts to a few tens of teraelectronvolts and can be fitted well by a power law with an index of 2.0.

For the leptonic scenario of HESS J1427−608, we compare the fitted parameters in Table 2 with those in the second class mentioned above, in Figure 6. And we find that the total energies of electrons of these SNRs are on the order of $\sim 10^{47}$–10^{48} erg, and the fitting result of HESS J1427−608 is also in coincidence with that under the assumption of distance being 8 kpc. However, the fitting magnetic field strength of HESS J1427−608 is at least two times lower than that of other SNRs, which may be attributed to variations in the progenitor and its environment. However, the X-ray flux is dominated by a central bright source instead of a shell structure of other SNRs. The model predicts a sharp cutoff beyond the HESS energy range, which can be tested with future CTA observations.

For the hadronic scenario, the parameters in our model are compared with SNRs whose γ-ray emissions are expected to be dominated by π^0 decay. The total energy of protons of HESS J1427−608, $W_p \approx 1 \times 10^{51}\ (n/1.0\,\mathrm{cm}^{-3})^{-1}\ (d/8.0\,\mathrm{kpc})^2$ erg, is significantly higher than the typical energy of particles, assuming that $\sim$10% of the supernova kinetic energy of $\sim 10^{51}$ erg is transferred to the energy of particles. On the one hand, this source may be left over from a hypernova explosion, which releases a substantially higher energy than typical supernova. On the other hand, a much higher value of W_p depending on the gas density and the distance means that HESS J1427−608 may be closer or the ambient environment of this source may be denser. Compared with the first class of SNRs, also known as SNRs interacting with molecular clouds leading to prominent thermal X-ray emissions, the X-ray emission from HESS J1427−608 is dominated by the nonthermal process. The absence of a shell structure in the X-ray band for HESS J1427−608 and no adjacent SNRs or molecular clouds found around it make it distinct from others, although several dark clouds are reported near the direction of HESS J1427−608 in the SIMBAD database.[7] In addition, the flat γ-ray spectrum of HESS J1427−608 from gigaelectronvolts to a few tens of teraelectronvolts is also significantly different from that of the first class of SNRs but is similar to that of the third class of SNRs, especially Tycho, which also emits nonthermal X-rays. For HESS J1427−608, the fitting cutoff energy of $\sim$350 TeV or even 1 PeV for protons is about one order of magnitude higher than the values of most SNRs, which suggests that HESS J1427−608 is a promising PeV CR accelerator (PeVatron). However, the absence of a shell structure in the X-ray band and the weak radio emission are also challenging to this possible origin.

3.3.2. PWN

The γ-ray emission from PWNe is dominated by the ICS process (Abdo et al. 2010a, 2010d). Fujinaga et al. (2013) discussed the PWN hypothesis of HESS J1427−608 with the X-ray and TeV data and indicated that a simple one-zone model with a magnetic field strength of about 5 μG would roughly explain the SED, and our result is consistent with that. Our GeV data, in combination with the flux upper limit in the radio band, however, favor a more complex broken power-law model. In addition, Vorster et al. (2013) also modeled the multiwavelength data of HESS J1427−608 as a PWN. The fitting parameters of the leptonic scenario listed in Table 2 are comparable with that of PWN Vela-X (Abdo et al. 2010d).

The X-ray, GeV, and TeV luminosities of HESS J1427−608 are $L_{\mathrm{X}}(2\text{–}10\ \mathrm{keV}) = 7 \times 10^{33}(d/8\,\mathrm{kpc})^2$ erg s^{-1}, $L_{\mathrm{GeV}}(>10\ \mathrm{GeV}) = 5.21 \times 10^{34}(d/8\,\mathrm{kpc})^2$ erg s^{-1}, and $L_{\mathrm{TeV}}(1\text{–}30\ \mathrm{TeV}) = 4.18 \times 10^{34}(d/8\,\mathrm{kpc})^2$ erg s^{-1} (Aharonian et al.

[7] http://simbad.u-strasbg.fr/simbad/

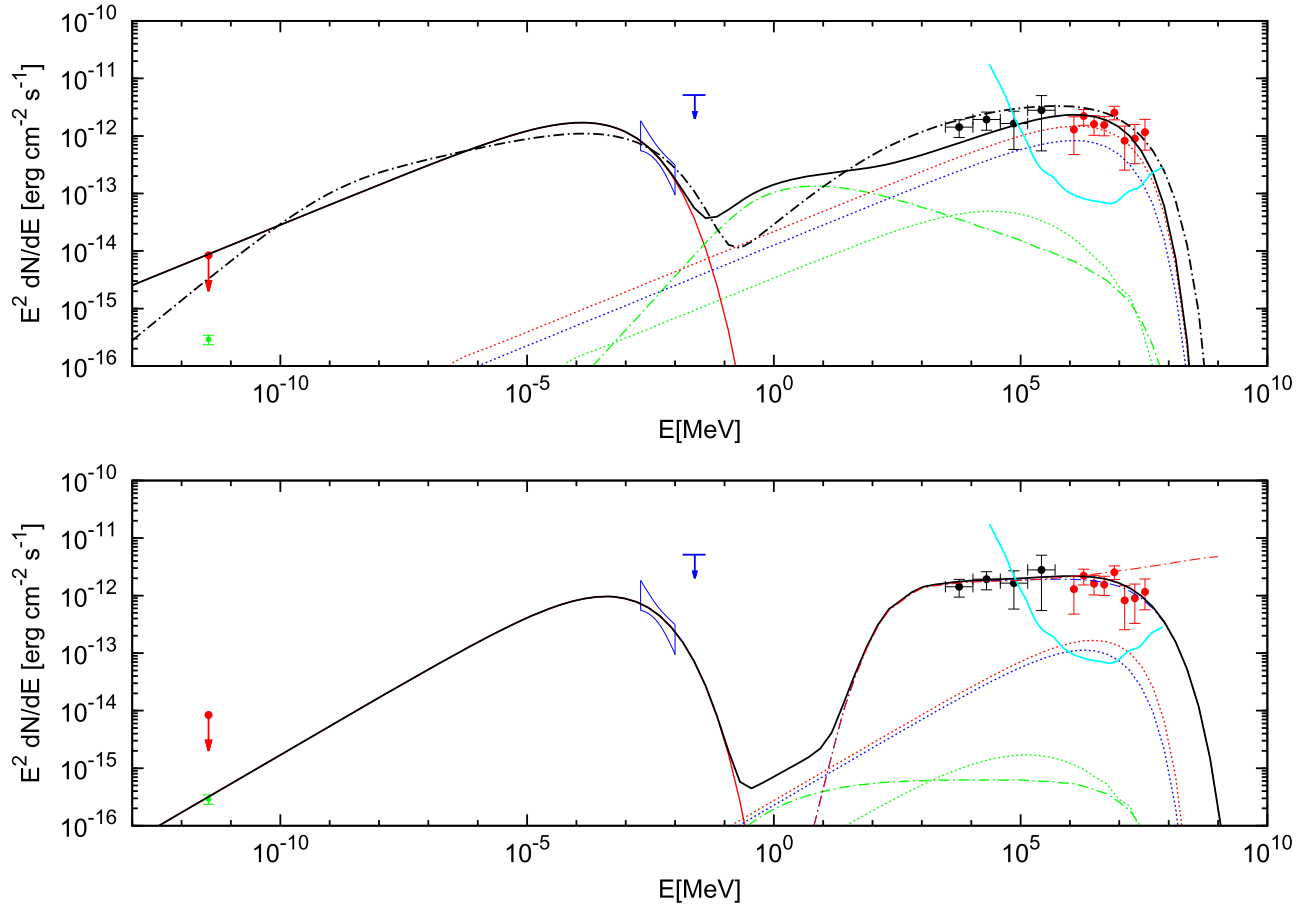

Figure 5. Multiwavelength SED of HESS J1427−608. The green point is the radio flux of MGPS J142755−605038 (Murphy et al. 2007), and the red arrow shows the upper limit recalculated based on the size of MGPS J142755−605038 and HESS J1427−608. The X-ray data marked by the blue butterfly and arrow are taken from *Suzaku* observation (Fujinaga et al. 2013). The top panel is for the leptonic scenario, and the bottom one is for the hadronic scenario. The radio and X-ray emissions are dominated by a synchrotron component, shown as a red solid curve. The γ-ray emission is mainly modeled by different contributions, including π^0 decay (blue dot-dashed), bremsstrahlung (green dot-dashed), and ICS (dotted) components. The ICS includes three components from the CMB (blue), infrared (red), and optical (green) radiation fields. The black solid line represents the sum of different radiation components. The cyan curve shows the differential sensitivity of CTA (100 hr; Funk et al. 2013). The black dot-dashed line in the top panel denotes the sum of different radiation components produced by the electrons with a broken power-law distribution, and the red dot-dashed line in the bottom panel represents the π^0 decay component for a proton distribution without a high-energy cutoff.

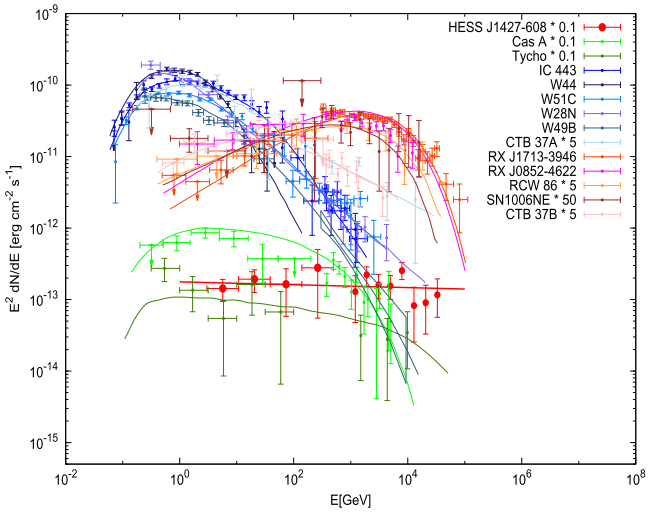

Figure 6. Typical γ-ray SED for several of the most prominent SNRs and HESS J1427−608. The energy fluxes of several sources with relatively flat spectra are scaled downward by one order of magnitude for the sake of clarity.

2008a), respectively. These estimated luminosities are within the range of known PWNe or PWN candidates that have emissions in the X-ray and γ-ray bands (Mattana et al. 2009; Acero et al. 2013). The ratio between the X-ray and γ-ray luminosities is approximately equal to 1, which is consistent with the value of magnetic field strength in our fitting, and the value of about 5 μG is also typical for PWNe. Mattana et al. (2009) and Acero et al. (2013) studied a large sample of PWNe and derived the relations among $F_{\rm TeV}/F_{\rm X}$, $L_{\rm GeV}/L_{\rm X}$, spin-down energy $\dot{E}$, and characteristic age τ_c of the pulsars. The ratio between the GeV and X-ray luminosities of HESS J1427−608 is estimated to be about 7.44, and according to these relations in Mattana et al. (2009) and Acero et al. (2013), the values of $\dot{E}$ and τ_c of a pulsar to power HESS J1427−608 are suggested to be $\sim$6.5 $\times$ 10^{36} erg s^{-1} and 11 kyr, respectively. The values of $\dot{E}$ and τ_c are typical for Vela-like pulsars.

For the PWN hypothesis, the discussion above indicates that a Vela-like pulsar may exist in the vicinity of HESS J1427−608. The detection of a pulsar near HESS J1427−608 will strongly support such a scenario. Therefore, future observations, especially a pulsation search in the radio and other

energy bands, are of great importance in addressing this hypothesis.

4. CONCLUSION

We investigate more than 7 years of data from the *Fermi*-LAT in the direction of the unidentified TeV source HESS J1427−608. A point source is detected with a significance of $\sim 5.5\sigma$. This GeV source is positionally coincident with HESS J1427−608, and the GeV spectrum can connect with the TeV spectrum smoothly. These facts suggest that this source is very likely the GeV counterpart of HESS J1427−608.

We collect multiwavelength data to constrain the radiation model of HESS J1427−608. Both the leptonic and hadronic scenarios can fit the SED. At present it is difficult to exclude either one considering the large uncertainties of the data. A remarkable spectral feature of this source is its E^{-2} spectrum over four decades of energies without obvious cutoff. This is unique among all currently detected γ-ray sources. If CR protons are responsible for the γ-ray emission, the highest energy of protons should exceed a few hundred teraelectronvolts and even petaelectronvolts. This makes HESS J1427−608 a promising PeV CR accelerator (PeVatron).

Unfortunately, the nature of HESS J1427−608 is not clear yet. Either an SNR or a PWN seems to be plausible. The low strength of the magnetic field and the absence of a shell structure in the X-ray band indicate that HESS J1427−608 may be a PWN rather than an SNR. However, its flat γ-ray spectrum in a wide energy range is closer to that of some SNRs but different from typical PWNe. Further multiwavelength observations, in the radio and VHE γ-rays, are crucial to ultimately understanding its nature. In particular, the precise measurements of the γ-ray energy spectrum up to hundreds of TeV energies by, for example, the CTA, will crucially test its PeVatron nature.

This work is supported by the Natural Science Foundation of Jiangsu Province of China (No. BK2014102SBZ0140), the 973 Programme of China (No. 2013CB837000), the National Natural Science Foundation of China (Nos. 11433009, 11233001 and 11303098), the Strategic Priority Research Program, the Emergence of Cosmological Structures, of the Chinese Academy (No. XDB09000000), and the 100 Talents program of the Chinese Academy of Sciences.

REFERENCES

Abdo, A. A., Ackermann, M., Ajello, M., et al. (Fermi LAT Collaboration) 2009, ApJL, 706, L1
Abdo, A. A., Ackermann, M., Ajello, M., et al. (Fermi LAT Collaboration) 2010a, ApJ, 708, 1254
Abdo, A. A., Ackermann, M., Ajello, M., et al. (Fermi LAT Collaboration) 2010b, ApJL, 710, L92
Abdo, A. A., Ackermann, M., Ajello, M., et al. (Fermi LAT Collaboration) 2010c, ApJ, 712, 459
Abdo, A. A., Ackermann, M., Ajello, M., et al. (Fermi LAT Collaboration) 2010d, ApJ, 713, 146
Abdo, A. A., Ackermann, M., Ajello, M., et al. (Fermi LAT Collaboration) 2010e, Sci, 327, 1103
Abdo, A. A., Ackermann, M., Ajello, M., et al. (Fermi LAT Collaboration) 2010f, ApJ, 718, 348
Abdo, A. A., Ackermann, M., Ajello, M., et al. (Fermi LAT Collaboration) 2010g, ApJ, 722, 1303
Abdo, A. A., Ackermann, M., Ajello, M., et al. (Fermi LAT Collaboration) 2011, ApJ, 734, 28
Acero, F., Ackermann, M., Ajello, M., et al. (Fermi LAT Collaboration) 2013, ApJ, 773, 77
Acero, F., Ackermann, M., Ajello, M., et al. (Fermi LAT Collaboration) 2015, ApJS, 218, 23
Acero, F., Aharonian, F., Akhperjanian, A. G., et al. 2010, A&A, 516, A62
Ackermann, M., Ajello, M., Allafort, A., et al. (Fermi LAT Collaboration) 2013, Sci, 339, 807
Aharonian, F., Akhperjanian, A. G., Aye, K. M., et al. (HESS Collaboration) 2005, Sci, 307, 1938
Aharonian, F., Akhperjanian, A. G., Barres de Almeida, U., et al. (HESS Collaboration) 2008a, A&A, 477, 353
Aharonian, F., Akhperjanian, A. G., Bazer-Bachi, A. R., et al. (HESS Collaboration) 2006a, ApJ, 636, 777
Aharonian, F., Akhperjanian, A. G., Bazer-Bachi, A. R., et al. (HESS Collaboration) 2006b, A&A, 456, 245
Aharonian, F., Akhperjanian, A. G., Bazer-Bachi, A. R., et al. (HESS Collaboration) 2008b, A&A, 481, 401
Araya, M., & Frutos, F. 2012, MNRAS, 425, 2810
Brandt, T. J. & Fermi-LAT Collaboration 2013, AdSpR, 51, 247
Brun, F., de Naurois, M., Hofmann, W., et al. 2011, arXiv:1104.5003
Fujinaga, T., Mori, K., Bamba, A., et al. 2013, PASJ, 65, 61
Funk, S. 2015, ARNPS, 65, 245
Funk, S., Hinton, J. A. & CTA Consortium 2013, APh, 43, 348
Giordano, F., Naumann-Godo, M., Ballet, J., et al. 2012, ApJL, 744, L2
Green, D. A. 2014, BASI, 42, 47
Hui, C., Yeung, P. K. H., Ng, C. W., et al. 2016, MNRAS, 457, 4262
Jogler, T., & Funk, S. 2016, ApJ, 816, 100
Mattana, F., Falanga, M., Götz, D., et al. 2009, ApJ, 694, 12
Morlino, G., & Caprioli, D. 2012, A&A, 538, A81
Murphy, T., Mauch, T., Green, A., et al. 2007, MNRAS, 382, 382
Nolan, P. L., Abdo, A. A., Ackermann, M., et al. 2012, ApJS, 199, 31
Porter, T. A., Moskalenko, I. V., & Strong, A. W. 2006, ApJL, 648, L29
Tanaka, T., Allafort, A., Ballet, J., et al. 2011, ApJL, 740, L51
Vorster, M. J., Tibolla, O., Ferreira, S. E. S., & Kaufmann, S. 2013, ApJ, 773, 139
Xin, Y.-L., Liang, Y.-F., Li, X., et al. 2016, ApJ, 817, 64
Xing, Y., Wang, Z., Zhang, X., & Chen, Y. 2016, ApJ, 823, 44
Yuan, Q., Huang, X., Liu, S., & Zhang, B. 2014, ApJL, 785, L22
Yuan, Q., Liu, S., Fan, Z., Bi, X., & Fryer, C. 2011, ApJ, 735, 120
Yuan, Y., Funk, S., Jóhannesson, G., et al. 2013, ApJ, 779, 117
Zeng, H.-D., Xin, Y.-L., Liu, S.-M., et al. 2016, arXiv:1611.07564
Zhang, J.-L., Bi, X.-J., & Hu, H.-B. 2006, A&A, 449, 641
Zhang, X., Chen, Y., Li, H., & Zhou, X. 2013, MNRAS, 429, L25